Continuous air purification by front flow photocatalytic reactor: Modelling of the influence of mass transfer step under simulated real conditions

Youcef Serhane, Nacer Belkessa, Abdelkrim Bouzaza, Dominique Wolbert, Aymen Amin Assadi

To cite this version:

Youcef Serhane, Nacer Belkessa, Abdelkrim Bouzaza, Dominique Wolbert, Aymen Amin Assadi. Continuous air purification by front flow photocatalytic reactor: Modelling of the influence of mass transfer step under simulated real conditions. Chemosphere, 2022, 295, pp.133809. 10.1016/j.chemosphere.2022.133809 . hal-03594101

HAL Id: hal-03594101
https://hal.science/hal-03594101v1

Submitted on 22 Mar 2022

Continuous air purification by front flow photocatalytic reactor: Modelling of the Influence of mass transfer step under simulated real conditions

Youcef Serhane[a], Nacer Belkessa[a], Abdelkrim Bouzaza[a], Dominique Wolbert[a],
Aymen Amin Assadi[a,*]

[a] Univ Rennes, École Nationale Supérieure de Chimie de Rennes, CNRS, ISCR (Institut des Sciences Chimiques de Rennes) – UMR 6226, F-35000 Rennes, France

*Corresponding author. Tel: +33(0)223238152, Fax: +33(0)223238120,

E-mail: Aymen.assadi@ensc-rennes.fr

ABSTRACT

In this work, a solution for the treatment of toxic gases based on a photocatalytic process using TiO_2 coated on a cellulosic support, has been investigated. Here, cyclohexane was chosen as the reference for testing its removal efficiency via a continuous front flow reactor as type A anti-gas filters. The photocatalytic support was firstly characterized by EDX, to confirm its elemental composition. Then, the experiments were carried out, starting with a batch reactor in order to evaluate the degradation efficiency of the photocatalytic media, as well as the monitoring of the photocatalytic process which allowed the establishing of a carbon mass balance corresponding to the stoichiometric number of our target pollutant. The transition to a continuous treatment with a front flow reactor aims to highlight the influence of the input concentration (0.29 – 1.78 mM m^{-3}) under different flow rates (12, 18 and 36 L min^{-1}). The relative humidity effect was also investigated (from 5 to 90% of humidity) where an optimum rate was obtained around 35 to 45%. In addition, the mineralization rate was monitored. The major rates obtained were for a cyclohexane input concentration of 0.29 mM m^{-3} in wet condition (38%) at an air flow rate of 18 L min^{-1}, where the CO_2 selectivity reached 77% for an abatement of 62%. In order to understand the limiting steps of the photocatalytic process, a model considering the reactor geometry and the hydraulic flow was developed. The obtained results showed that the mass transfer must be considered in the photocatalytic process for a continuous treatment. The Langmuir-Hinshelwood bimolecular model was also developed to represent the influence of the humidity.

Keywords

Air treatment, Photocatalytic front flow reactor, kinetic modelling, mass transfer.

1. Introduction

Air pollution is increasingly a major concern, the result of pollution caused by many factors, often of human origin. Faced with the adverse effects of this pollution, both on human health and the environment, scientists are still trying to find new techniques and processes to remedy the problem. Advanced oxidation processes, such as photocatalysis, are a promising process for this application because of its ability to mineralize many volatile organic compounds (VOCs) into CO_2, H_2O and other by-products (Malayeri et al., 2019; Talaiekhozani et al., 2021). The design of the photocatalytic reactor for environmental applications, including air treatment, is both a major and difficult task because of the different factors involved in the process namely, the pollutant, the catalyst as well as the photon flux. (Boyjoo et al., 2017; Sundar and Kanmani, 2020; He et al., 2021).

Among the continuous photocatalytic reactors are with front flow configurations. This configuration, even if it is less developed in the laboratory, remains interesting because it allows to have a compact reactor able to work at high flow rates by promoting mass transfer whatever the contact time is sacrificed (Vuong., 2011; Debono et al., 2018; Malayeri et al., 2021; Oliveira De Brito Lira et al., 2021). It is well known that tangential flow reactors are most common in the literature, where the residence times is longer but the limitation by mass transfer is more important (Dalida and Ramoso, 2017; Sundar and Kanmani, 2020). For continuous flow reactors, it is generally assumed that they operate under ideal plug flow configuration, and for which, degradation rates are determined ignoring dispersion/diffusion phenomena (Zhong et al., 2017; Salvadores et al., 2020). It has even been reported that when the flow rate is high enough (turbulent flow regime) and the length to diameter ratio of the reactor is significant, the axial dispersion is minimal; therefore, the flow in the reactor can be considered as plug flow (Davis, M.E. and R.J., 2012). The performance of the photocatalytic reactor is often interpreted by two successive phenomena: the transport of the mass of pollutants to the catalyst surface and their elimination by photocatalytic reaction. Most studies (Amrheinet al., 2012; Malayeri et al., 2019) have assumed that the process is limited by kinetic reaction and mass transfer is often ignored in photocatalysis studies, the reason is that they try to focus more on the catalyst activity and its efficiency, even though knowledge of the mass transfer phenomenon plays an essential role in interpreting the experimental results and scaling-up the photocatalytic reactor.

In this study, the photocatalytic performance in a front flow reactor was highlighted for the abatement of cyclohexane, which is defined as a reference for testing the effectiveness of type "A" gas filters (INRS., 2011, 2019; Vuong., 2017; Chauveau, 2018). The aim is to establish a kinetic analysis, which presents a powerful tool for the evaluation of the catalytic properties of the experimental device and the reaction rate in the photocatalytic oxidation process. This is done by determining the main factors affecting the catalytic performance or the kinetic parameters of the photoreaction, namely the adsorption capacity and the oxidation capacity of the photocatalysts. Langmuir-Hinshelwood (L-H) model, which remains the most widely used kinetic expression, was adopted to formulate the rate of reaction.

The novelty of this study is the development of a model, which considers both the aeraulic of the flow through the residence time distribution (RTD) determination and the mass transfer limitations. Since the relative humidity influences the efficiency of the photocatalytic process, it was therefore essential to consider water molecules in the expression of the reaction rate. Consequently, the Langmuir-Hinshelwood (L-H) biomolecular model was developed to consider the effect of competitions.

2. Materials and methods

In this part, the various commercial catalytic supports used as well as the polluted air generation systems adopted, then the air treatment devices, the analytical techniques, the methodology used are exposed

2.1. Photocatalytic support

The photocatalytic support used is supplied by the Ahlstrom company under the reference Alhström 1049. It is a non-woven fabric made of synthetic and natural cellulose fibers, where a winding press process has been used to coat them with a mixture of TiO_2 and SiO_2, whose masses per square meter are equal to 16 and 13.3 g m^{-2} respectively. The colloidal silica used has a specific surface area of about 700 m² g^{-1}, with elementary particles of 20-30 nm in diameter. It acts as an inorganic binder, resistant to UV radiation and photocatalysis, transparent to UV and protecting the TiO_2 fibers. The TiO_2 used for this deposit is a PC-500, marketed by Millennium. The elemental crystals are between 5 and 10 nm in size, with an anatase crystal structure (> 99%) and an S_{BET} surface area of approximately 320 m² g^{-1}. The energy dispersive X-ray (EDX) technique (Fig. S1) allows the determination of elemental composition of the cellulose media by highlighting these different elements such as: titanium and oxygen, aluminum was a residual compound from the mechanical processing of the textiles, and silicon corresponded to the silica deposit.

2.2. Pollutant studied

The cyclohexane used is supplied by Sigma-Aldrich in liquid form (purity> 98%). It is then volatilized to obtain the desired gas concentrations. Its main characteristics are given in Table S1.

2.3. Reactor and experimental set-up

2.3.1. Batch reactor

The batch reactor is shown in Fig. S2 and contains a central tube for the lamp and ports for sampling/analysis. It is approximately 40 cm high and has a volume of 1.5 L. The catalytic support, with a surface area of 81 cm^2, giving a mass of TiO_2 of 0.13 g, is deposited on inner wall of the reactor. To generate pollution in the reactor, the pollutant is injected as liquid drops which then evaporate. A magnetic stirrer and a magnetic barrel make it possible to homogenize the gases. The fluorescent UV lamp (Philips PL-L 24W/10/4P) used is purchased from Lum'On (France). This lamp has a wavelength spectrum of 310-390 nm with a maximum of UV intensity at 365 nm. A VLX-3W radiometer equipped with a CX-365 cell is used to measure UV intensity.

A control system based on oxygen analyzer, temperature, humidity and CO_2 sensors was installed on the batch reactor. These sensors were connected to an Arduino board allowing online acquisition of experimental data.

2.3.2. Continuous process

The front flow photocatalytic reactor (P50) illustrated in Fig. 1 is formed by four mountable stainless-steel test chambers with a passage section of 0.01 m^2 and a total volume of about 4 L. The first part is used for the main inlet of the flow of water vapor, air, injection of pollutants, and sampling for analysis before handling. The second part contained four photocatalytic media (4 m x 0.01 m of surface giving 0.64 g of TiO_2) and two Philips UV-A lamps (model PLS 9W / 10). The intensity of the light incident at 365 nm on the surface of the catalyst is 20 W m^{-2}. The last element allows the sampling for analysis after treatment and the exit of the air flow. The air leaving the reactor is evacuated under a hood.

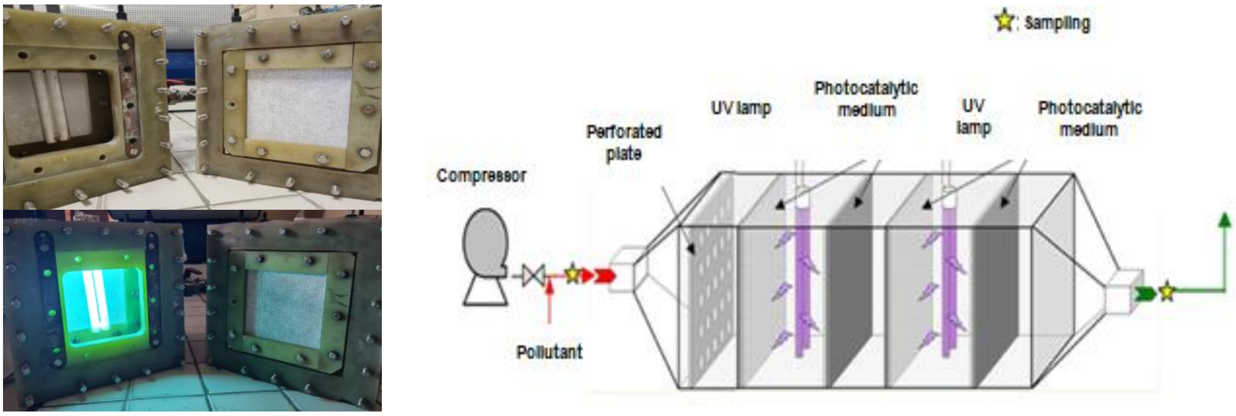

Figure 1: Photo and Schematic of P50, front flow continuous photocatalytic reactor

2.3.2.1. Experimental setup

The dry air coming from the network is the carrier gas, controlled by a valve and estimated using a Gallus G4 gas meter of the Itrón brand. The flow rates tested is equivalent to human respiratory flow rates 13, 18 and 36 L min^{-1}. These flow rates correspond to contact times of 18, 13 and 7 ms respectively. To humidify the air, a bubbler was installed in the circuit containing water to achieve humidity ranges of 30-90%. The pollutant is injected continuously in liquid form by a syringe / syringe pump combination. A heating tape, placed in the injection zone to facilitate the volatilization of the pollutant and a static mixer makes it possible to homogenize the effluent upstream of the photoreactor. Two septas downstream and upstream of the photoreactor make it possible to sample the outlet and inlet gas with a syringe (Fig. S3).

2.3.2.2. Analytic tools

The concentration of cyclohexane was measured by a Thermo electron corporation gas chromatography (Focus GC) using a flame ionization detector (FID) and an FFAP column (length = 25 m and internal diameter = 0,32 mm). Nitrogen was used as a carrier gas. The temperature conditions of the oven, the injection chamber and the detector were, respectively, 50, 190 and 190 °C. The analysis was performed by direct manual sampling with a 500 µl syringe and injection into the GC. The calibration was carried out by evaporating different quantities of cyclohexane on a closed bottle. The correlation of the pollutant with a peak area of GC-FID as a function of its concentration was carried out. Operation is done by Azur™ software.

The CO_2 was analyzed by a Fourier transform infrared spectrophotometer (FTIR) from Environment SA (MIR 9000H).

The overall rate of photocatalytic degradation is an important factor in evaluating VOC's removal performance. VOC's removal efficiency is defined:

$$RE\ (\%) = \frac{[\mathrm{VOCs}]in - [\mathrm{VOCs}]out}{[\mathrm{VOCs}]in}\ 100\ \% \qquad (1)$$

The overall rate of photocatalytic degradation of cyclohexane is calculated as:

$$\mathrm{r} = \left(\frac{\mathrm{Q}}{\mathrm{S}}\right)\left(\frac{[\mathrm{VOCs}]in}{100}\right) RE\ (\%) \qquad (2)$$

Where $[\mathrm{VOCs}]in$ and $[\mathrm{VOCs}]out$ are respectively the inlet and outlet pollutant concentration (mM m^{-3}), Q is the volumetric flow rate (L min^{-1}) and S the mean surface of the support (m^2).

The overall selectivity of CO_2 can be a useful parameter in evaluating the performance of the photocatalytic reactor with respect to the removal of VOCs. It makes it possible to estimate the rate of mineralization, that is to say the final reaction step of the process. The global selectivity of CO_2 is expressed as follows

$$SCO_2\,(\%) = \frac{[CO_2]out - [CO_2]in}{N_C\ \ RE\ (\%)\ [\mathrm{VOCs}]in}\ 10^4 \qquad (3)$$

Where $[CO_2]_{in}$ and $[CO_2]_{out}$ refer respectively to the concentration of carbon dioxide at the air inlet and outlet (mM m^{-3}). The number N_c represents the stoichiometric coefficient of the overall degradation reaction (in our case, it is equal to 6).

2.3.2.3. Experimental procedure

With batch reactor, different amounts of pollutants are injected in liquid form with a syringe. The stirrer is turned on and the reactor is covered with an opaque bag. When adsorption equilibrium is reached (approximately 30 min), the UV lamp is turned on and samples are taken regularly (every 5 min), to monitor changes in concentrations. The samples are taken with a 500 µl syringe and are directly analyzed by gas chromatography with flame ionization detection.

Concerning the P50, once the adsorption process reaches equilibrium (depending on the concentration), as indicated by an identical input / output Volatile Organic Compound concentration, the UV lighting is turned on, a transient period precedes a steady state phase which is established when the concentration of pollutant at the outlet becomes constant.

After completing the experiments, the reactor is rinsed under UV lighting for 1 h in ambient air. No deactivation observed during the entire operating time.

3. Results and discussions

3.1.1. Photocatalytic kinetic degradation with using the batch reactor

The performance of the TiO_2 on cellulosic media was investigated in terms of degradation efficiency, degradation and elimination rates at different pollutant concentrations and UV intensity.

Fig. 2a and 2b show the evolution of the concentrations of cyclohexane during photocatalytic reactions under different UV irradiations as a function of time at different input concentrations. From Fig. 2a and by comparing the degradation rate for the different input concentrations at about 20 min. It is observed that the degradation rate decreases proportionally as the initial concentration increases (from 70% for 1.78 mM m^{-3} to 52.5% for 6.53 mM m^{-3}). The same trend is always observed when UV intensity is higher (Fig. 2b). This can be interpreted by the unavailability of active sites (Elfalleh et al., 2017).

The results show that at low input concentration, degradation follows pseudo-first order kinetics where degradation is proportional to the input concentration. This can be explained by the fact that all the active sites are not occupied and an increase in the concentration generates a higher surface coverage which implies a better rate of degradation. It also means that the chemical reaction is the limiting step in the process. The results show that light intensity is also an important parameter, which influences the performance of photocatalytic processes. Indeed, the increase in UV intensity seems to be significant on the generation of the active site (Herrmann, 2010; Palau et al., 2012). This can be explained by the fact that as the UV intensity increases, the number of photons hitting the surface of the photocatalyst can increase and lead to more electrons and holes (Brosillon et al., 2008; Assadi et al., 2014).

Thus, the results show a similar behaviour to what is reported in the literature with other pollutants such as toluene, decane and trichloroethylene (TCE) (Debono et al., 2017), Ethylene (Stroe and Rosendahl, 2019), also 2,3-butane-dione (Abidi et al., 2020).

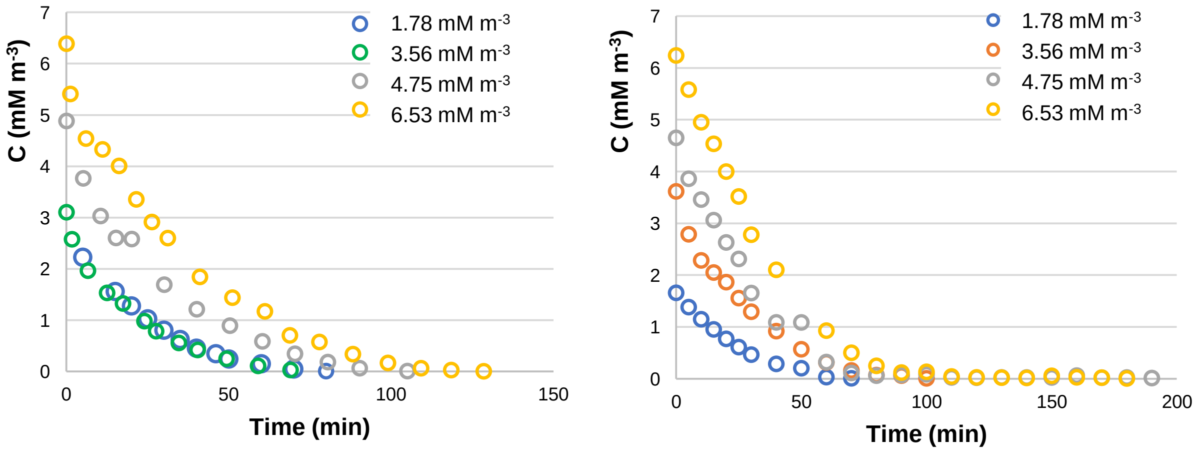

a

b

Figure 2: Kinetics of cyclohexane degradation in a batch reactor at: (a) UV intensity = 1.5 W m^{-2} and (b) UV intensity = 12 W m^{-2}

The degradation kinetics are generally represented by Langmuir – Hinshelwood (L-H) model. The latter is defined by the following equation at initial degradation rate (Abidi et al., 2020) .

$$r_0 = \frac{kKC_0}{1+\mathrm{K}C_0} \qquad (4)$$

$$\text{Or} \quad \frac{1}{r_0} = \frac{1}{\mathrm{kK}}\frac{1}{C_0} + \frac{1}{\mathrm{k}} \qquad (5)$$

where r_0 is the initial reaction rate (mM m^{-3} s^{-1}), k the reaction rate constant (mM m^{-3} s^{-1}) et K is the adsorption constant (m^3 mM^{-1}).

Initial reaction rate can be obtained from the initial slope of the curve C=f(time) where the influence of by-products is supposed to be negligible. The results are shown in Fig. S4.

By plotting $r_0^{-1} = f(C_0^{-1})$ (Fig. S5) and from the values of the slope and the intercept, the value of the Langmuir-Hinshelwood constants for the two intensity were determined and summarized in table S2.

The results showed that the increase in light intensity leads to a faster elimination of the VOC, reflected by an increase in the kinetic constant from 0.0027 to 0.0051 mM m^{-3} s^{-1} for I= 1.5 and 12 W m^{-2} respectively. It is well known that the degradation rate is linked to the activation of the catalyst. A power relation law is usually used ($k_{app} = k_0.I^{\alpha}$) where α is around 0.5 for intermediate intensities. In our case α seems to be equal to 0.25. This is mainly due to the recombination of the e^- / h^+ pairs versus charge transfer. (Brosillon et al., 2008; Queffeulou et al., 2010; Assadi et al., 2014).

3.1.2. Photocatalytic degradation mechanism of cyclohexane

There is still a need to identify intermediate products of photocatalytic degradation that could be a potential tool to explore the intrinsic kinetics of photocatalytic oxidation. The literature has shown that the gaseous by-products of cyclohexane degradation cannot be identified by GC analysis (Geng et al., 2013). To identify them, other methods have been used where it has been shown that the main degradation intermediates are cyclohexanol and cyclohexanone and the final degradation products are water and CO_2 (Selishchev et al., 2012; Geng et al., 2013; Sannino et al., 2013).

From the above works, a follow-up experiment to monitor the removal of cyclohexane. (millimole per cubic meter), accumulation of CO_2 (millimole per cubic meter) and H_2O (absolute humidity ‘grams per cubic meter of air') in the batch reactor was performed. The results are shown in Fig. S6.

The results show that when the UV lamp is tuned ON and the photocatalytic process start, a clear change in the amount of CO_2 and H_2O formed in proportion to the degradation of cyclohexane is observed.

The result of the balance between the quantity of CO_2 formed at the end of the degradation process ($[CO_2]_{Formed}$ = 130.1 mM m^{-3}) relative to the concentration of Cyclohexane introduced initially ($[\text{Cyclohexane}]_{initial}$ = 23.3 mM m^{-3}), shows that 1 mole of Cyclohexane gives an equivalent of 6 moles of CO_2. This carbon balance corresponds to the stoichiometric number of Cyclohexane.

The carbon balance was naturally accompanied by an evolution of the quantity of H_2O from 7.8 g $m^{-3}{}_{air}$ up to 13.45 g $m^{-3}{}_{air}$ which makes an equivalent production of 5.65 g $m^{-3}{}_{air}$ of Water. It should be noted that the quantity of O_2 was sufficient throughout the degradation process.

The results are also consistent with the literature (Zhong et al., 2015; Xu et al., 2022, 2021) regarding the degradation mechanism of cyclohexane. Where initially cyclohexane is oxidized by h^+ to produce cyclohexyl radicals ($C_6H_{11}°$) (Eq. 6). the latter react with O_2 to produce a peroxy radical ($C_6H_{11}OO°$) (Eq. 7). The reaction of the peroxy radicals ($C_6H_{11}OO°$) (Eq. 8) produces cyclohexanone ($C_6H_{10}O$) and cyclohexanol ($C_6H_{11}OH$) which will be oxidized by h^+ in turn to produce cyclohexanone (Eq. 9).

$$C_6H_{12} + h^+ \rightarrow C_6H_{11}° + H^+ \quad (6)$$

$$C_6H_{11}° + O_2 \rightarrow C_6H_{11}OO° \quad (7)$$

$$C_6H_{11}OO° + C_6H_{11}OO° \rightarrow C_6H_{11}OH + C_6H_{10}O + O_2 \quad (8)$$

$$C_6H_{11}OH + 2\ h^+ \rightarrow C_6H_{10}O + 2\ H^+ \qquad (9)$$

Cyclohexanone is also produced via the reduction of the radial $C_6H_{11}OO°$ by e^-. This reaction is accompanied mainly by the production of water (Eq. 10).

$$C_6H_{11}OO° + e^- + 2\ H^+ \rightarrow C_6H_{10}O + H_2O \qquad (10)$$

After all the steps of cyclohexanone production, it is then decomposed to CO_2. Even though the detailed decomposition mechanism is not yet clear, our results fit perfectly with the one suggested by the literature (Shiraishi et al., 2017) where h^+ and the reaction with $O_2^{°-}$ are involved in the oxidation mechanism of cyclohexanone (Eq. 11).

$$C_6H_{10}O + h^+ + O_2^{°-} \rightarrow \text{decomposition} \rightarrow CO_2 \qquad (11)$$

3.2. Photocatalytic degradation in continuous reactor

3.2.1. Effect of flow rate and inlet concentration

The inlet concentration of cyclohexane is varied between 0.29 and 1.78 mM m^{-3}, in order to understand its influence on the performance of the photocatalytic reactor. The removal efficiency of cyclohexane at different input concentrations with different flow rates is shown in Fig. 3.

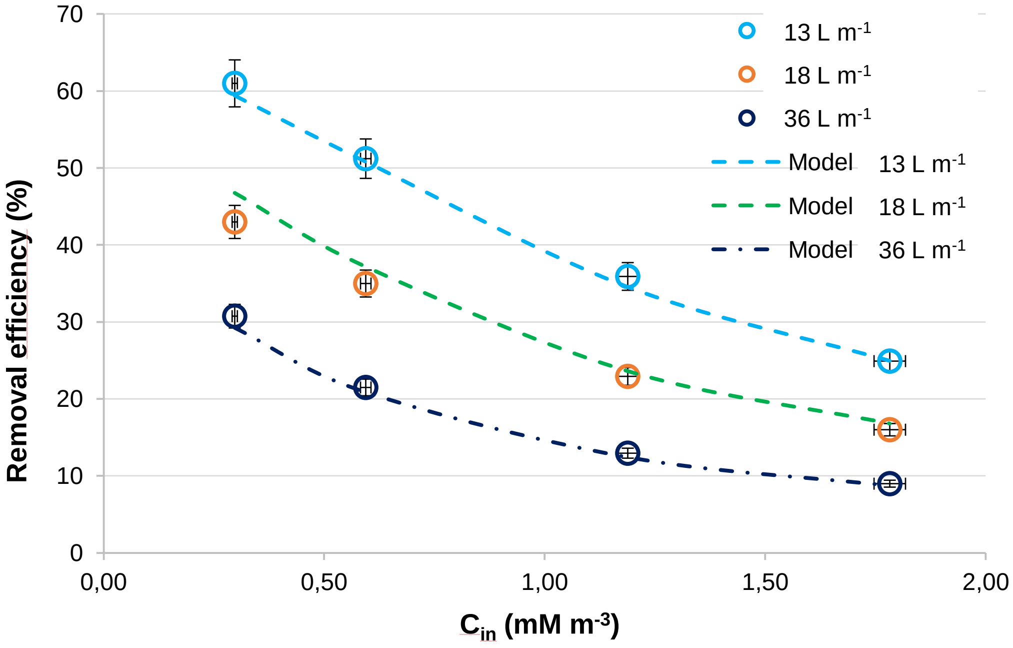

Figure 3: Influence of the inlet concentration and the flow rate on the elimination of cyclohexane (HR = 5%, UV Intensity = 20 W m^{-2}, T=20 ± 2 °C). Model taking into account the mass transfer step

For a given flowrate, at a higher concentration of pollutants, the rate of degradation will tend towards a limit (RE ~ 9% for 1.78 mM m^{-3}), which may be linked to a limitation by the chemical reaction step due to the unavailability of active sites (Abou Saoud et al., 2017, 2018). It can also be noted that the removal efficiency of cyclohexane decreases with increasing flow rate, this is due to a reduction in the contact time between the compound and the catalytic active sites. in line with what was obtained when studying the impact of residence time on the removal efficiency of Methyl Ethyl Ketone (MEK) and toluene (Mamaghani et al., 2018), also, Propionic acid and Benzene (Zadi et al., 2020).

3.2.2. Effect of relative humidity

In order to study the effect of relative humidity on the efficiency of continuous photocatalysis with the P50 reactor, it was necessary to apply a relative humidity range between 5 % and 87 % at 20 ± 2 °C under the same concentrations mentioned above. The variation in the elimination efficiency of cyclohexane at different inlet concentrations and under different relative humidity is illustrated in Fig. 4.

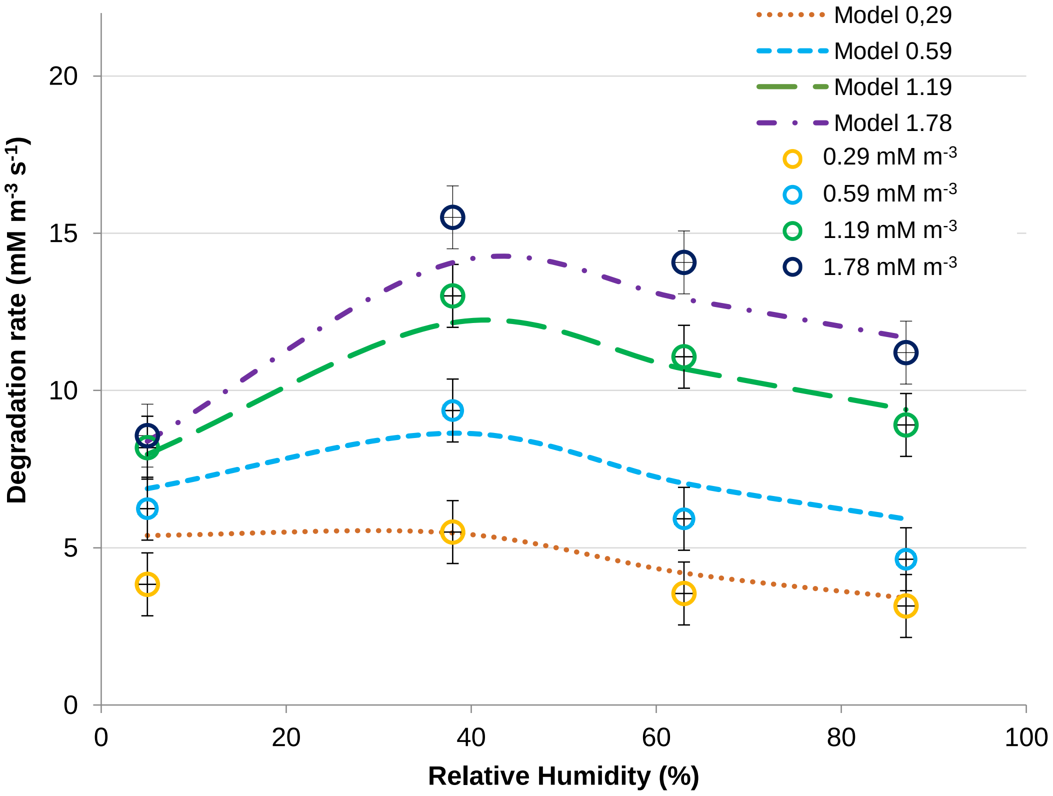

Figure 4: Influence of relative humidity on the elimination of cyclohexane and the Bimolecular model curves (Q = 18 L min^{-1}, UV intensity= 20 W m^{-2}, T= 20 ± 2 °C).

Firstly, the elimination efficiency of cyclohexane increases with increase of relative humidity, which could be explained by the generation of hydroxyl radicals. An optimum is observed, and thus a permanent decrease in the elimination efficiency occurs. In fact, the more the humidity increases, the more there is deactivation of the active sites of the catalyst due to competitive adsorption on the active sites of the catalyst between the molecules of water vapor (H_2O) and Cyclohexane (Chen et al., 2011; Vandenbroucke et al., 2011; Zadi et al., 2020; Zhang et al., 2020).

3.2.3. Selectivity of CO_2

Fig. 5a shows the dependence of the selectivity versus the inlet concentration of Cyclohexane. As expected the input concentration exerts a significant influence on the amount of CO_2 Selectivity, which decreases by increasing the concentration of the pollutant. This is due to the fact that there is less availability of active sites on the surface of the photocatalyst.(Assadi et al., 2014; Zadi et al., 2020). This behaviour also confirms that the process is limited by the availability of active sites.

The increase of the inlet gas flow rate leads also to a decrease in mineralization rate (Fig.5b). This can be explained by the fact that the contact time is insufficient which will not allow by-products to be degraded. Moreover the competitive phenomena of the by-products formed towards the active sites reduces the selectivity (Assadi et al., 2012).

Under humid conditions (Fig. 5c), it’s clearly voiced the influence of humidity on the CO_2 selectivity for an inlet concentration of 1.78 mM m^{-3} where (i) the rate of mineralization increases from 22.2% to 34.2% when RH increases from 5 to 38%.

This improvement is due to the increase in water molecules which helps generate OH° hydroxyl radicals (according to Eq. (12) and (13).

$$H_2O + e^- \rightarrow H^\circ + OH^\circ + e^- \qquad (12)$$

$$H_2O + h^+ \rightarrow OH^\circ + H^+ \qquad (13)$$

(ii) On the other hand, a decrease in the selectivity is observed (29.3% compared to 34.2%) when RH varies from 38 to 63%). This is due to competition between Water vapor / Cyclohexane on the surface of the catalyst. These results are in agreement with those reported by literature concerning the oxidation of some VOCs (Assadi et al., 2013; Martinez et al., 2014; Zadi et al., 2018).

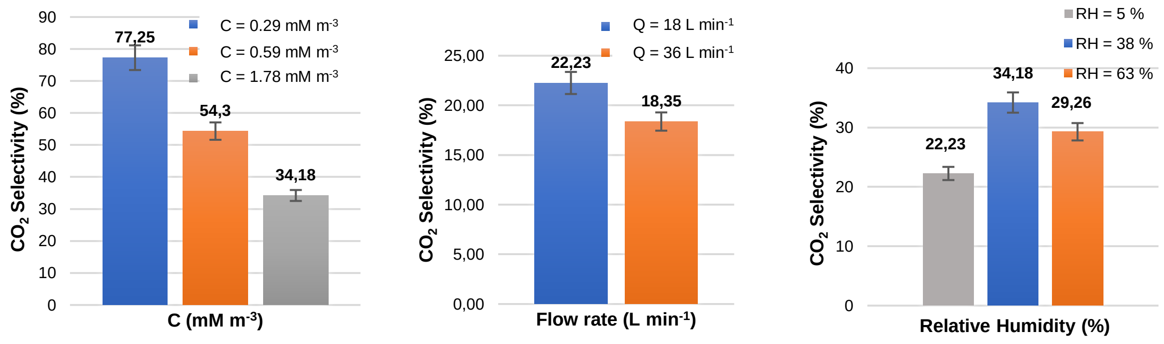

a b c

Figure 5: Variation of the CO_2's selectivity (%) with a) the Inlet concentration of Cyclohexane ($Q = 18$ L min^{-1}, RH= 38 ± 2 %, UV intensity= 20 W m^{-2}, T= 20 ± 2 C°), b) the flow rate (C = 1.78 mM m^{-3}, *HR = 5 %, intensity= 20 W m^{-2}, T= 20 ± 2 C°) and c) at different Relative Humidity (C= 1,78* mM m^{-3}*, Q = 18 L min^{-1}, UV intensity= 20 W m^{-2}, T= 20 ± 2 C°)*

3.2.4. Modeling of degradation kinetics and influence of mass transfer, comparison between the constants with batch reactor

The objective of the following part is to propose a model to describe the experimental observed kinetics. This kinetic model will consider the surface reaction and mass transfer step. The degradation kinetics of monocomponents in heterogeneous photocatalytic treatments is often represented by the Langmuir - Hinshelwood model (Queffeulou et al., 2010; Assadi et al., 2015; Muñoz-Batista and Luque, 2021)

Firstly, the aerodynamic conditions of the P50 reactor have to be determined.

A residence time distribution (RTD) experiment was performed. To characterize the gas flow pattern in the photoreactor, and in order to simulate the pulse function (Dirac delta function) a tracer (carbon dioxide) was injected for a very short time interval (Gao et al., 2012; Bérard et al., 2021; Rodrigues, 2021). The output CO_2 concentration is measured using an infrared sensor connected to an Arduino board allowing direct reading as a function of time on a PC. The stock model tanks were used to describe the response of the system. RTD experiments revealed that our flow-through reactor can be likened to a cascade of 18 elementary continuously stirred tank reactors (Fig.S7). Thus our experimental reactor can be considered as a plug flow reactor (Jafarikojour et al., 2014).

3.2.4.1. Model without mass transfer

In this part, only the surface reaction step is considered, that is to say that the mass transfer is neglected, to describe the gas-solid phase reaction for heterogeneous photocatalysis. Assuming that the mass transfer is not the limiting step and that the effect of the intermediate product is negligible, then the reaction rate can be expressed as:

$$r = k\frac{KC}{1+KC} \tag{14}$$

Where r is the degradation rate (mM m^{-3} s^{-1}), K is the adsorption constant (m^3 mM^{-1}), k is the reaction constant (with the same unit as the rate of degradation), and C is the concentration of the contaminant (mM m^{-3}). In such a model, the adsorption and desorption steps are kinetically negligible compared to the oxidative reaction step. The pollutant adsorption rate is greater than any by-product adsorption rate and the binding products do not interact with each other or modify the initial activity of the reactive sites.

The reactor is plug flow in a stationary state, the continuous degradation of pollutants along the axial direction should not be ignored. The continuity equation for a contaminant is written:

$$u\frac{dC}{dz} = -r \qquad (15)$$

where z represents the axial position in the photoreactor. After rearrangement, integration of Eq. (15) for the entire length of the reactor L leads to (Queffeulou et al., 2010; Assadi et al., 2015):

$$\frac{ln\left(C^{in}/\,C^{out}\right)}{C^{in}-C^{out}} = \frac{k_{app}KL}{u}\frac{1}{C^{in}-C^{out}} \text{ - } K \qquad (16)$$

Where u is the superficial velocity of the gas (m s^{-1}). The L-H constants k and K are determined by fitting the results for each flow and contaminant with the linear equation. The cross-correlation coefficient is defined as the covariance of the pair k and K divided by the standard deviation of each parameter k and K (Table S3 and Fig. S8).

The model correlates quite well with the experimental data. However, and despite a high R^2, the values of k and K with this frontal flow reactor vary by varying the flow rate. This variation is less significant compared to the results obtained with tangential reactors, in particular those obtained during the study of (Assadi et al., 2012), whether in the treatment of trimethylamine in an annular reactor or for the treatment of isovaleraldehyde with annular and planar reactors (Assadi et al., 2016) where it has been shown that the mass transfer was more important. This does not prevent the conclusion of the dependence of these constants on the flow rate. Therefore, it seems more appropriate to propose a new model where the mass transfer step is considered.

3.2.4.2. Model with mass transfer step

The limitation of the internal mass transfer step is not considered due to superficial reaction sites (Vincent et al., 2008; Assadi et al., 2012; Palau et al., 2012; Assadi et al., 2013; Assadi et al., 2015; Costa et al., 2017). Therefore, only the external mass transfer is considered. Thus, the mass transfer constant k_m which depends only to the flow regime is considered.

The overall mass balances of the pollutant on the solid and gas phases in a continuous piston reactor leads to the following equations (Yang et al., 2007; Queffeulou et al., 2010; Assadi et al., 2016):

In the gas phase:

$$u\frac{dC}{\mathrm{dz}} + k_m a_v (C - C^s) = 0 \qquad (17)$$

In solid phase:

$$k_m a_v (C - C^s) = \frac{k_{app} K C^s}{1 + K C^s} \qquad (18)$$

where C and C^s are respectively the gas phase concentrations of the overall and average surface area of VOC (mM m^{-3}), k_m is the mass transfer coefficient (m s^{-1}) and a_v is the average surface area per unit volume of the reactor (m^2 m^{-3}).

The mass transfer term k_m can be estimated by semi-empirical Williamson expression. Correlation used exclusively for frontal flow (Petit., 2007; Vuong., 2011):

$$k_m = 0.44\, u\, Re^{-0.31}\, Sc^{-0.58}, if\!: \; 125 \le Re \le 5000 \qquad (19)$$

Where ($Sc = \frac{\mu}{\rho\, D_{mol}}$) and ($Re = \frac{d\, \rho\, u}{\mu}$) are Schmidt and Reynolds numbers, respectively. With the dynamic viscosity of the gas μ (Pa s), the gaseous density ρ (kg m^{-3}) and the equivalent diameter d (m).

The molecular diffusion coefficient D$_{mol}$ is necessary for the calculation of the Schmidt number. In the case of gas phase applications, the Fuller, Schettler and Giddings relationship has been used. (Perry., 1997).

$$D_{mol} = \frac{10^{-3}\sqrt{\frac{M+29}{M\,.29}}}{(20{,}1^{1/3}+{V_m}^{1/3})^2}\ \frac{T^{1{,}75}}{P_{atm}} \qquad (20)$$

where P is the pressure of the gas flow (Pa), T the absolute temperature (K). V$_m$ is the molecular volume of the gas (m^3 M^{-1}), and M is the molecular mass of the pollutant (g M^{-1}). The molecular diffusion coefficient D$_{mol}$ is 0.0509 cm^2 s^{-1}.

The key values are summarized in Table S4.

The Reynolds number varies from 1500 to 4600 for flow rates varying from 13 to 36 L min^{-1} respectively. The flow regime thus confirms that the mass transfer step may be considered.

To solve Eq. (17) and (18), Maple software is used to develop a system under the series method. In addition, it was established that the second-order development is sufficiently precise (Assadi et al., 2013; Abidi et al., 2021). In the Eq. (21), the two unknown parameters are k and K. They are determined by numerical resolution with the Excel Solver.

$$C^{in} - C^{out} = \frac{L k_m a_v}{2u}\left[C^{in} + \frac{1}{\mathrm{K}} + \frac{k}{k_m a_v} - \sqrt{\left(-C^{in} + \frac{1}{\mathrm{K}} + \frac{k}{k_m a_v}\right)^2 + \frac{4C^{in}}{\mathrm{K}}}\ \right] \qquad (21)$$

The model allows a good description of the experimental results (Fig. 3 and 6). The obtained values of k and K are respectively 0,025 mM m^{-3} s^{-1} and 7,122 m^3 mM^{-1}. Obviously, when transfer is neglected, the reaction rate constant (k) is slightly overestimated. Instead, the adsorption constant (K) is underestimated.

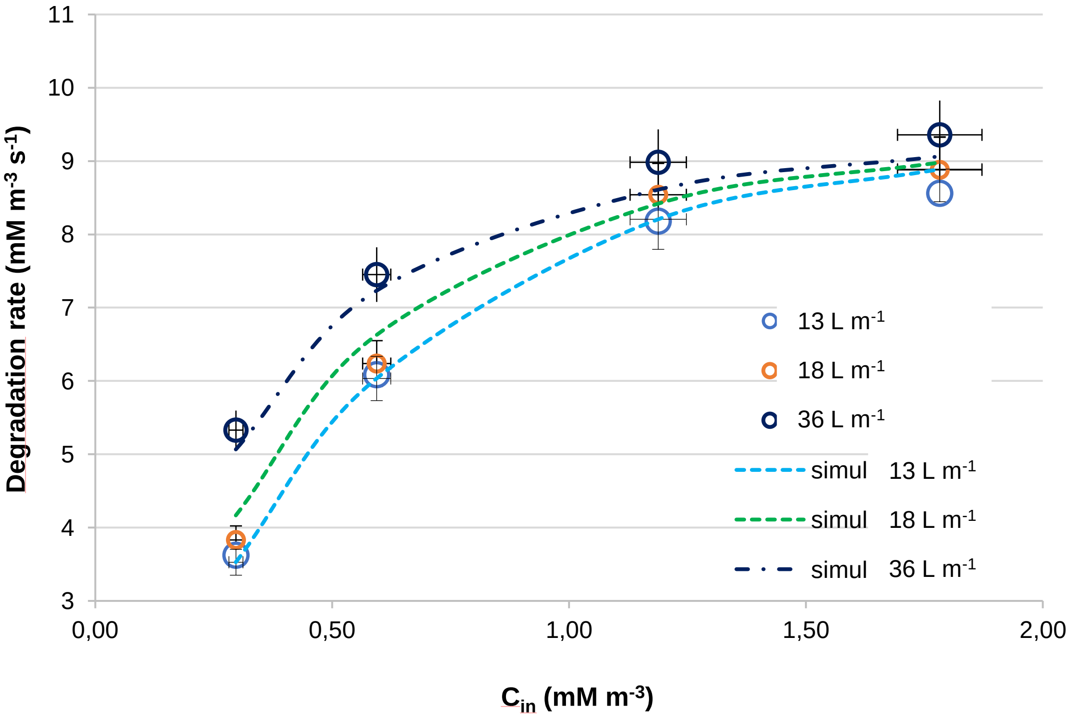

Figure 6: Influence of the inlet concentration and the flow rate on the degradation rate of cyclohexane (Q = 18 L min^{-1}, UV intensity= 20 W m^{-2}, T= 20 ± 2 °C). Model taking into account the mass transfer step

In addition, it is interesting to note that these constants are not flow dependent. The influence of the flow regime is fully integrated by the k_m parameter. Indeed, the separation between the mass transfer and the chemical reaction steps is obtained. It is also noted that the constants determined in this study depend mainly on the geometry of the reactor, taking into consideration the hydraulics of the flow of the pollutant stream. (Qiao et al., 2012; Assadi et al., 2013; Abidi et al., 2021).

It can also be noted that unlike the effect of the flow rate on the pollutant removal efficiency, when the flow rate increases, the mass transfer rate increases between the gas and the surface of the photocatalyst, which leads to an increase in the reaction rate (Assadi et al., 2013).

Taking into consideration the amount of the catalyst (TiO_2) in the process of Cyclohexane treatment in the batch reactor and the continuous reactor P50 under the same UV intensity, the kinetic constants (k) can be compared, knowing that for the continuous reactor the mass transfer step has to be considered.

The Values of kinetic constants determined with L - H model in batch (0.13 g_{TiO2}) and continuous reactor P50 by considering Mass transfer (0.64 g_{TiO2}) are 0.0392 mM m^{-3} s^{-1} $m_{TiO2}{}^{-1}$ and 0.0391 mM m^{-3} s^{-1} $m_{TiO2}{}^{-1}$, respectively. These constants are of the same order. This means that the mass transfer step is negligible for batch reactor due to good homogeneity of the gas phase (mixing). It's obviously shown that model taking account the mass transfer step, allows the access to the real reaction kinetics.

3.3. Effect of the relative humidity on the degradation rate

To correlate the experimental data, the Langmuir - Hinshelwood bimolecular model can be used (L. Zhang et al., 2020), considering the VOC-Water system as a binary mixture. The degradation kinetics can be expressed by:

$$r_A = k_A F_A F_w \tag{22}$$

Where $$F_A = \frac{K_A C_A}{(1+K_A C_A+K_w C_w)} \tag{23}$$

and $$F_w = \frac{K'_w C_w}{(1+K'_A C_A+kK'_w C_w)} \tag{24}$$

therefore $$r_A = k_A \frac{K_A C_A}{(1+K_A C_A+K_w C_w)} \times \frac{K'_w C_w}{(1+K'_A C_A+kK'_w C_w)} \tag{25}$$

Where C_w is the concentration of water vapor, K_w is the Langmuir adsorption constant of water, K'_A et K'_w are respectively the competitive adsorption constant of the pollutant and water. Constants k_A and K_A are taken from the previous study, where the mass transfer was considered under dry air conditions.

K'_A (m^3 mM^{-1})	0,011
K'_w (m^3 mM^{-1})	0,0133
K_w (m^3 mM^{-1})	0,0129
R^2 (%)	99

Table 1: Values of kinetic constants determined with the bimolecular model L – H

All model constants are determined numerically using the Excel solver. The Langmuir-Hinshelwood bimolecular model Eq. (25) correlates well the experimental results and that the validity of this approach is confirmed (Table 1, Fig. 4).

The result shows an optimum humidity for photocatalytic degradation at about 35-45% at different input concentrations. This result is similar to that obtained with our previous works on isovaleraldehyde, trimethylamine, chloroform and glutaraldehyde (Assadi et al., 2012; Abidi et al., 2021), even on BTEX compounds (Martinez et al., 2014) as well as Methyl Ethyl Ketone (Malayeri et al., 2021).

4. Conclusion

The elimination of cyclohexane was studied in two reactors: batch and continuous reactor. The influence of the inlet concentration and the flow rate on the performance of the reactor was studied. The increase in these two parameters leads to a decrease in the efficiency of conversion and elimination of the pollutant. On the other hand, the complex effect of relative humidity on the elimination of Cyclohexane has been studied. The presence of water vapor is beneficial at moderate concentrations due to the formation of OH• radicals which contribute to increased degradation.

Moreover, the influence of mass transfer was estimated by testing two models based on the Langmuir-Hinshelwood approach. With considering the limitation of mass transfer, the constants are more realistic and not dependent on flow rates. A bimolecular L-H kinetic model including the effect of relative humidity and the mass transfer step has been highlighted. The model was satisfactory in correlating the experimental data.

References:

Abidi, M., Hajjaji, A., Bouzaza, A., Lamaa, L., Peruchon, L., Brochier, C., Rtimi, S., Wolbert, D., Bessais, B., Amin Assadi, A., 2021. Modeling of indoor air treatment using an innovative photocatalytic luminous textile: reactor compactness and mass transfer enhancement. Chem. Eng. J. 132636. https://doi.org/10.1016/j.cej.2021.132636

Abidi, M., Hajjaji, A., Bouzaza, A., Trablesi, K., Makhlouf, H., Rtimi, S., Assadi, A.A., Bessais, B., 2020. Simultaneous removal of bacteria and volatile organic compounds on Cu2O-NPs decorated TiO2 nanotubes: Competition effect and kinetic studies. J. Photochem. Photobiol. A Chem. 400. https://doi.org/10.1016/j.jphotochem.2020.112722

Abou Saoud, W., Assadi, A.A., Guiza, M., Bouzaza, A., Aboussaoud, W., Ouederni, A., Soutrel, I., Wolbert, D., Rtimi, S., 2017. Study of synergetic effect, catalytic poisoning and regeneration using dielectric barrier discharge and photocatalysis in a continuous reactor: Abatement of pollutants in air mixture system. Appl. Catal. B Environ. 213, 53–61. https://doi.org/10.1016/j.apcatb.2017.05.012

Abou Saoud, W., Assadi, A.A., Guiza, M., Bouzaza, A., Aboussaoud, W., Soutrel, I., Ouederni, A., Wolbert, D., Rtimi, S., 2018. Abatement of ammonia and butyraldehyde under non-thermal plasma and photocatalysis: Oxidation processes for the removal of mixture pollutants at pilot scale. Chem. Eng. J. 344, 165–172. https://doi.org/10.1016/j.cej.2018.03.068

Amrhein, K., D, Stephan., 2012. Photocatalytic building materials and methods of mea- surement, Ultra-High Performance Concrete and Nanotechnology in Construction. Proceedings of Hipermat 2012. 3rd International Symposium on UHPC and Nanotechnology for High Performance Construction Materials, kassel university press GmbH, 2012.

Assadi, A.A., Abdelkrim, B., Dominique, W., 2016. Kinetic Modeling of VOC Photocatalytic Degradation Using a Process at Different Reactor Configurations and Scales. Int. J. Chem. React. Eng. 14, 395–405. https://doi.org/10.1515/ijcre-2015-0003

Assadi, A.A., Bouzaza, A., Lemasle, M., Wolbert, D., 2015. Acceleration of Trimethylamine Removal Process Under Synergistic Effect of Photocatalytic Oxidation and Surface Discharge Plasma Reactor. Can. J. Chem. Eng. 93, 1239–1246. https://doi.org/10.1002/cjce.22211

Assadi, A.A., Bouzaza, A., Wolbert, D., 2012. Photocatalytic oxidation of trimethylamine and isovaleraldehyde in an annular reactor: Influence of the mass transfer and the relative humidity. J. Photochem. Photobiol. A Chem. 236, 61–69. https://doi.org/10.1016/j.jphotochem.2012.03.020

Assadi, A.A., Bouzaza, A., Wolbert, D., Petit, P., 2014. Isovaleraldehyde elimination by UV/TiO<inf>2</inf> photocatalysis: comparative study of the process at different reactors configurations and scales. Environ. Sci. Pollut. Res. 21, 11178–11188. https://doi.org/10.1007/s11356-014-2603-7

Assadi, A.A., Palau, J., Bouzaza, A., Wolbert, D., 2013. Modeling of a continuous photocatalytic reactor for isovaleraldehyde oxidation: Effect of different operating parameters and chemical degradation pathway. Chem. Eng. Res. Des. 91, 1307–1316. https://doi.org/10.1016/j.cherd.2013.02.020

Bérard, A., Blais, B., Patience, G.S., 2021. Residence time distribution in fluidized beds: diffusion, dispersion, and adsorption. Adv. Powder Technol. 32, 1677–1687. https://doi.org/10.1016/j.apt.2021.03.019

Boyjoo, Y., Sun, H., Liu, J., Pareek, V.K., Wang, S., 2017. A review on photocatalysis for air treatment: From catalyst development to reactor design. Chem. Eng. J. 310, 537–559. https://doi.org/10.1016/j.cej.2016.06.090

Brosillon, S., Lhomme, L., Vallet, C., Bouzaza, A., Wolbert, D., 2008. Gas phase photocatalysis and liquid phase photocatalysis: Interdependence and influence of substrate concentration and photon flow on degradation reaction kinetics. Appl. Catal. B Environ. 78, 232–241. https://doi.org/10.1016/j.apcatb.2007.09.011

Chauveau, R., 2018. Modélisation multiparamètre du phénomène d'adsorption : détermination du temps de percée des cartouches de masques à gaz to cite this version : HAL Id : tel-01751295 soutenance et mis à disposition de l'ensemble de la Contact : ddoc-theses-contact@uni.

Chen, J., Li, G., He, Z., An, T., 2011. Adsorption and degradation of model volatile organic compounds by a combined titania-montmorillonite-silica photocatalyst. J. Hazard. Mater. 190, 416–423. https://doi.org/10.1016/j.jhazmat.2011.03.064

Costa, G., Assadi, A.A., Gharib-Abou Ghaida, S., Bouzaza, A., Wolbert, D., 2017. Study of butyraldehyde degradation and by-products formation by using a surface plasma discharge in pilot scale: Process modeling and simulation of relative humidity effect. Chem. Eng. J. 307, 785–792. https://doi.org/10.1016/j.cej.2016.07.099

Dalida, M.L.P., Ramoso, P.D., 2017. Design, Mass Transfer Studies, and Optimization of an Air-Sparged Tubular Photocatalytic Reactor for the Degradation of Methylene Blue. Int. J. Chem. Eng. Appl. 8, 5–9. https://doi.org/10.18178/ijcea.2017.8.1.622

Davis, M.E. and R.J. Davis, Fundamentals of chemical reaction engineering. 2012: Chaptre 3 - Reactors for mesuring reaction rate, page 76.

Debono, O., Gaudion, V., Redon, N., Locoge, N., Thevenet, F., 2018. Photocatalytic treatment of VOC industrial emissions: IPA removal using a sensor-instrumented reactor. Chem. Eng. J. 353, 394–409. https://doi.org/10.1016/j.cej.2018.07.151

Debono, O., Hequet, V., Le Coq, L., Locoge, N., Thevenet, F., 2017. VOC ternary mixture effect on ppb level photocatalytic oxidation: Removal kinetic, reaction intermediates and mineralization. Appl. Catal. B Environ. 218, 359–369. https://doi.org/10.1016/j.apcatb.2017.06.070

Elfalleh, W., Assadi, A.A., Bouzaza, A., Wolbert, D., Kiwi, J., Rtimi, S., 2017. Innovative and stable TiO2 supported catalytic surfaces removing aldehydes under UV-light irradiation. J. Photochem. Photobiol. A Chem. 343, 96–102. https://doi.org/10.1016/j.jphotochem.2017.04.029

Gao, Y., Muzzio, F.J., Ierapetritou, M.G., 2012. A review of the Residence Time Distribution (RTD) applications in solid unit operations. Powder Technol. 228, 416–423.

https://doi.org/10.1016/j.powtec.2012.05.060

Geng, Q., Wang, Q., Zhang, Y., Wang, L., Wang, H., 2013. Photocatalytic degradation intrinsic kinetics of gaseous cyclohexane in a fluidized bed photocatalytic reactor. Res. Chem. Intermed. 39, 1711–1726. https://doi.org/10.1007/s11164-012-0904-3

He, F., Jeon, W., Choi, W., 2021. Photocatalytic air purification mimicking the self-cleaning process of the atmosphere. Nat. Commun. 12, 10–13. https://doi.org/10.1038/s41467-021-22839-0

Herrmann, J.M., 2010. Photocatalysis fundamentals revisited to avoid several misconceptions. Appl. Catal. B Environ. 99, 461–468. https://doi.org/10.1016/j.apcatb.2010.05.012

Hunger, M., Hüsken, G., Brouwers, H.J.H., 2010. Photocatalytic degradation of air pollutants - From modeling to large scale application. Cem. Concr. Res. 40, 313–320. https://doi.org/10.1016/j.cemconres.2009.09.013

INRS, 2019. Appareils de protection respiratoire.

INRS, 2011. Les appareils de protection respiratoire. Choix et utilisation.

Jafarikojour, M., Sohrabi, M., Royaee, S.J., Rezaei, M., 2014. Residence time distribution analysis and kinetic study of toluene photo-degradation using a continuous immobilized photoreactor. RSC Adv. 4, 53097–53104. https://doi.org/10.1039/c4ra05239k

Malayeri, M., Haghighat, F., Lee, C.S., 2021. Kinetic modeling of the photocatalytic degradation of methyl ethyl ketone in air for a continuous-flow reactor. Chem. Eng. J. 404, 126602. https://doi.org/10.1016/j.cej.2020.126602

Malayeri, M., Haghighat, F., Lee, C.S., 2019. Modeling of volatile organic compounds degradation by photocatalytic oxidation reactor in indoor air: A review. Build. Environ. 154, 309–323. https://doi.org/10.1016/j.buildenv.2019.02.023

Mamaghani, A.H., Haghighat, F., Lee, C.S., 2018. Photocatalytic degradation of VOCs on various commercial titanium dioxides: Impact of operating parameters on removal efficiency and by-products generation. Build. Environ. 138, 275–282. https://doi.org/10.1016/j.buildenv.2018.05.002

Martinez, T., Bertron, A., Escadeillas, G., Ringot, E., Simon, V., 2014. BTEX abatement by photocatalytic TiO2-bearing coatings applied tocement mortars. Build. Environ. 71, 186–192. https://doi.org/10.1016/j.buildenv.2013.10.004

Muñoz-Batista, M.J., Luque, R., 2021. Heterogeneous photocatalysis. ChemEngineering 5, 341–357. https://doi.org/10.3390/chemengineering5020026

Oliveira De Brito Lira, J., Riella, H.G., Padoin, N., Soares, C., 2021. An Overview of Photoreactors and Computational Modeling for the Intensification of Photocatalytic Processes in the Gas-Phase: State-of-Art. J. Environ. Chem. Eng. 9. https://doi.org/10.1016/j.jece.2021.105068

Palau, J., Penya-Roja, J.M., Gabaldón, C., Álvarez-Hornos, F.J., Martínez-Soria, V., 2012. Effect of pre-treatments based on UV photocatalysis and photo-oxidation on toluene biofiltration performance. J. Chem. Technol. Biotechnol. 87, 65–72. https://doi.org/10.1002/jctb.2683

Perry, R.H., Green D., Maloney J.O., 1997. Perry’s Chemical Engineers’s Handbook, seventh ed., Mc-Graw Hill, New York. 5-48. HEAT AND MASS TRANSFER -TABLE 5-14 Correlations of Diffusivities for Gases.

Petit, N., 2007. Couplage des procédés d'adsorption sur charbon actif et de photocatalyse TiO2/UV pour l'élimination des composés organiques volatils. Tableau 5 : Corrélations semi-empiriques pour accéder à k_f, page 43.

Qiao, Z., Wang, Z., Zhang, C., Yuan, S., Zhu, Y., Wang, J., 2012. PVAm–PIP/PS composite membrane with high performance for CO_2/N_2 separation. AIChE J. 59, 215–228. https://doi.org/10.1002/aic

Queffeulou, A., Geron, L., Schaer, E., 2010. Prediction of photocatalytic air purifier apparatus performances with a CFD approach using experimentally determined kinetic parameters. Chem. Eng. Sci. 65, 5067–5074. https://doi.org/10.1016/j.ces.2010.05.024

Rodrigues, A.E., 2021. Residence time distribution (RTD) revisited. Chem. Eng. Sci. 230. https://doi.org/10.1016/j.ces.2020.116188

Salvadores, F., Alfano, O.M., Ballari, M.M., 2020. Kinetic study of air treatment by photocatalytic paints under indoor radiation source: Influence of ambient conditions and photocatalyst content. Appl. Catal. B Environ. 268, 118694. https://doi.org/10.1016/j.apcatb.2020.118694

Sannino, D., Vaiano, V., Ciambelli, P., Murcia, J.J., Hidalgo, M.C., Navío, J.A., 2013. Gas-phase photocatalytic partial oxidation of cyclohexane to cyclohexanol and cyclohexanone on Au/TiO2 photocatalysts. J. Adv. Oxid. Technol. 16, 71–82. https://doi.org/10.1515/jaots-2013-0107

Selishchev, D.S., Kolinko, P.A., Kozlov, D. V., 2012. Influence of adsorption on the photocatalytic properties of TiO 2/AC composite materials in the acetone and cyclohexane vapor photooxidation reactions. J. Photochem. Photobiol. A Chem. 229, 11–19. https://doi.org/10.1016/j.jphotochem.2011.12.006

Shiraishi, Y., Shiota, S., Hirakawa, H., Tanaka, S., Ichikawa, S., Hirai, T., 2017. Titanium Dioxide/Reduced Graphene Oxide Hybrid Photocatalysts for Efficient and Selective Partial Oxidation of Cyclohexane. ACS Catal. 7, 293–300. https://doi.org/10.1021/acscatal.6b02611

Stroe, R.E., Rosendahl, L.A., 2019. Kinetic study of the photocatalytic oxidation of ethylene over TiO2 thin films. IOP Conf. Ser. Mater. Sci. Eng. 628. https://doi.org/10.1088/1757-899X/628/1/012009

Sundar, K.P., Kanmani, S., 2020. Progression of Photocatalytic reactors and it's comparison: A Review. Chem. Eng. Res. Des. 154, 135–150. https://doi.org/10.1016/j.cherd.2019.11.035

Talaiekhozani, A., Rezania, S., Kim, K.H., Sanaye, R., Amani, A.M., 2021. Recent advances in photocatalytic removal of organic and inorganic pollutants in air. J. Clean. Prod. 278, 123895. https://doi.org/10.1016/j.jclepro.2020.123895

Vandenbroucke, A.M., Morent, R., De Geyter, N., Leys, C., 2011. Non-thermal plasmas for non-catalytic and catalytic VOC abatement. J. Hazard. Mater. 195, 30–54. https://doi.org/10.1016/j.jhazmat.2011.08.060

Vincent, G., Marquaire, P.M., Zahraa, O., 2008. Abatement of volatile organic compounds using an annular photocatalytic reactor: Study of gaseous acetone. J. Photochem. Photobiol. A Chem. 197, 177–189. https://doi.org/10.1016/j.jphotochem.2007.12.021

Vuong, F., 2017. Modélisation du comportement des cartouches de protection respiratoire : exposition à des atmosphères complexes de vapeurs organiques et effet des cycles d ' utilisation François Vuong To cite this version : HAL Id : tel-01619367 soutenance et mis à dispo.

Vuong MD. Dépollution et désodorisons de l'air par photocatalyse assistée par adsorption sur charbon actif en réacteur à flux frontal continu et séquentiel. Thèse Univ. Rennes N° 4201, 2011. Tableau 16 : Corrélations empiriques pour accéder à $k_{f,}$ page 54.

Xu, G., Zhang, Ying, Peng, D., Sheng, D., Tian, Y., Ma, D., Zhang, Yao, 2021. Nitrogen-doped mixed-phase TiO2 with controllable phase junction as superior visible-light photocatalyst for selective oxidation of cyclohexane. Appl. Surf. Sci. 536. https://doi.org/10.1016/j.apsusc.2020.147953

Xu, G., Zhang, Ying, Peng, D., Sheng, D., Zhang, Yao, Tian, Y., Ma, D., 2022. MOF derived carbon modified porous TiO2 mixed-phase junction with efficient visible-light photocatalysis for cyclohexane oxidation. Mater. Res. Bull. 146. https://doi.org/10.1016/j.materresbull.2021.111602

Yang, R., Zhang, Y., Xu, Q., Mo, J., 2007. A mass transfer based method for measuring the reaction coefficients of a photocatalyst. Atmos. Environ. 41, 1221–1229. https://doi.org/10.1016/j.atmosenv.2006.09.043

Zadi, T., Assadi, A.A., Nasrallah, N., Bouallouche, R., Tri, P.N., Bouzaza, A., Azizi, M.M., Maachi, R., Wolbert, D., 2018. Treatment of hospital indoor air by a hybrid system of combined plasma with photocatalysis: Case of trichloromethane. Chem. Eng. J. 349, 276–286. https://doi.org/10.1016/j.cej.2018.05.073

Zadi, T., Azizi, M., Nasrallah, N., Bouzaza, A., Maachi, R., Wolbert, D., Rtimi, S., Assadi, A.A., 2020. Indoor air treatment of refrigerated food chambers with synergetic association between cold plasma and photocatalysis: Process performance and photocatalytic poisoning. Chem. Eng. J. 382, 122951. https://doi.org/10.1016/j.cej.2019.122951

Zhang, G., Liu, Y., Hashisho, Z., Sun, Z., Zheng, S., Zhong, L., 2020. Adsorption and photocatalytic degradation performances of TiO2/diatomite composite for volatile organic compounds: Effects of key parameters. Appl. Surf. Sci. 525. https://doi.org/10.1016/j.apsusc.2020.146633

Zhang, L., Moralejo, C., Anderson, W.A., 2020. A review of the influence of humidity on photocatalytic decomposition of gaseous pollutants on TiO2-based catalysts. Can. J. Chem. Eng. 98, 263–273. https://doi.org/10.1002/cjce.23652

Zhong, L., Brancho, J.J., Batterman, S., Bartlett, B.M., Godwin, C., 2017. Experimental and modeling study of visible light responsive photocatalytic oxidation (PCO) materials for toluene degradation. Appl. Catal. B Environ. 216, 122–132. https://doi.org/10.1016/j.apcatb.2017.05.047

Zhong, W., Qiao, T., Dai, J., Mao, L., Xu, Q., Zou, G., Liu, X., Yin, D., Zhao, F., 2015. Visible-light-responsive sulfated vanadium-doped TS-1 with hollow structure: Enhanced photocatalytic activity in selective oxidation of cyclohexane. J. Catal. 330, 208–221. https://doi.org/10.1016/j.jcat.2015.06.013